A multimodal scanner coupling XRF , UV–Vis–NIR photoluminescence and Vis–NIR–SWIR reflectance imaging spectroscopy for cultural heritage studies

R. Moreau, T. Calligaro, L. Pichon, B. Moignard, S. Hermon, I. Reiche

Development of a metaspectral scanner coupling XRF, UV-Vis-NIR Photoluminescence and Vis-NIR-SWIR Reflectance Imaging Spectroscopies

R. Moreau [1,2,3], T. Calligaro [2, 3, 4], L. Pichon [2, 4], B. Moignard [2, 4], S. Hermon[1], I. Reiche [2, 4]

1 APAC Labs, STARC, The Cyprus Institute, 2121 Aglantzia, Cyprus

2 Fédération de Recherche FR3506 New AGLAE, 75001 Paris, France

3 Chimie ParisTech, PSL University, CNRS, Institut de Recherche de Chimie de Paris (IRCP), UMR8247, 75005 Paris, France

4 Centre de Recherche et de Restauration des Musées de France, C2RMF, 75001 Paris, France

Abstract

Scanning X-Ray Fluorescence (MA-XRF), Reflectance Imaging Spectroscopy (RIS) and Luminescence Imaging Spectroscopy (LIS) are scientific imaging methods that are extensively used in the investigation and mapping of painted works of art materials in Cultural Heritage Science. Nevertheless, no instrument combining these three highly complementary methods for a simultaneous acquisition exists. In this paper, we present a scanning system combining MA-XRF, RIS and LIS, generating datacubes sharing the same spatial resolution and spatially aligned. The nature and processing of the obtained data is described, in particular their exploration and investigation through the coupled exploitation of datacubes. The operation of this instrument, which is the first to combine XRF with RIS and LIS mapping in an extended domain (400-2500 nm and 200-1000 nm respectively), is exemplified on an anonymous test painting, studied previously. A focus on a restored area of this painting allows to illustrates the complementarity of the three aforementioned methods, for the visualization and characterization of pigments, varnish and binders.

Keywords cultural heritage, instrumental development, Luminescence Imaging Spectroscopy (LIS), Reflectance Imaging Spectroscopy (RIS), scanning x-ray fluorescence (MA-XRF)

Introduction

The development of scanning X-Ray Fluorescence (MA-XRF) during the past decades has triggered a revolution in the scientific investigation of paintworks and many instruments were

developed by different institutions [1–7]. It has allowed the imaging of pigment distribution over large areas by means of associated elemental signatures[8], providing better insights in artist's painting materials, evidencing restoration areas and materials, and often revealing underlying and hidden compositions. Nevertheless, despite the short time spend per pixel for XRF data acquisition, MA-XRF scanning operation remains time consuming, requiring minutes to hours and sometimes days. Based on these observations, we developed a new MA-XRF system from a previous versatile scanning system designed by our group[6,9] to acquire during XRF scanning Reflectance Imaging Spectroscopy (RIS) in the Vis-NIR-SWIR range (400-2500 nm) and Luminescence Imaging Spectroscopy (LIS) in the UV-Vis-NIR range (200-1000 nm). The RIS and LIS spectroscopic imaging techniques are highly complementary to MA-XRF, and owing to their quick and non-destructive character, appears suitable for simultaneous implementation during MA-XRF acquisition[10–14]. The coupled exploitation of the signatures can help understanding the diverse materials generally encountered in cultural heritage paintworks, from pigments to binders, through varnishes and restoration materials, each technique complementing and corroborating each other. For instance, while the XRF elemental analysis generally allows identifying many pigments based on the elemental signature, reflectance in the Vis-NIR provides information on electronic bands[15,16], photoluminescence on crystal defects[17] while SWIR spectral features provides additional molecular information[18] (e.g. overtones of hydroxyl or carbonate bands) out of reach of the previous techniques. The datacubes generated with this instrument are naturally aligned in term of position and spatial resolution, facilitating coupled data processing, each analyzed point having its own XRF, RIS and LIS signatures. In addition, the orthoscopic imaging obtained (without optical deformation) also avoids the complex image corrections required to merge images from hyperspectral cameras. The instrument was designed to be carried on the field and to scan curved and non-vertical surfaces, and offers an attractive and cost-effective instrument in the field of heritage applications. The following sections describe the specification of the instruments, data processing steps and its application to a case study where the complementarity of the three presented methods is demonstrated.

Experimental

The present MA-XRF instrument is major evolution of a previous MA-XRF system whose details and operation are described elsewhere[6,9]. Using stepped-motor linear stages in a X/Y/Z stack (LTM80, OWIS GmbH) mounted on a sturdy geared head (Manfrotto 400), the instrument can map curved and non-vertical surfaces. It can be transported on the field, the analytical head weighting 20 kg and the entire instrument with all accessories 60 kg (Fig. 1).

The analytical head (Fig. 2) can scan an area extending up to 300 mm (horizontal) × 300 mm (vertical) × 120 mm (depth), following a raster scanning trajectory at constant speed. It is kept in focus during scanning using the Z movement and a telemetric laser pointer. The XRF section is built upon a microfocus X-ray generator (50 kV, 0.7 mA, Rh tube, iMOXS HELMUT-FISCHER) producing a sub-millimeter X-ray beam. The beam shape is defined either using a changeable collimator (∅ 0.2-0.8 mm) to produce a parallel beam for analysis at long working distance with broad excitation energy range (Rh L to 50 keV) or a using a polycapillary mini-lens for higher fluxes at shorter distances but narrower energy excitation range (4 keV- Rh K). X-rays are collected using a 70-mm² SDD X-ray detector (X123 FastSDD AMPTEK) with USB connection. XRF spectra are acquired on 512 channels, in order to maximize statistics per channel and to

minimize download time, and 1-µs shaping time allowing counts rates of 200 k counts/sec with acceptable pile-ups and short dead-times. During the dwell time of the XRF spectrum acquisition, four triggerable light sources (UV-C, UV-B, red and white lasers) are sequentially illuminating the probed spot and optical spectra in the 200-1000 nm range collected using a UV-Vis-NIR spectrometer. In parallel with these acquisitions, a XRF spectrum is acquired and the probed spot is continuously shined by an IR light source and the resulting reflectance spectrum in the 1000-2500 nm range is acquired using a dedicated SWIR spectrometer.

As shown in Figs. 2 and 3, UV illuminations are obtained using two LED sources: UV-C (250 nm, 11 nm FWHM, 1 mW optical power), UV-B (365 nm, 10 nm FWHM, 15 mW optical power). The UV-C LED integrating a ball lens directly illuminates the sample at close distance (15 mm) to compensate for its limited optical power. The UV-B illumination is transported through an UV-solarization resistant fiber and focused using a quartz lens located at 45° in the vertical plane. Both UV illuminations are filtered out using a UV band pass filter to block spurious emission of the UV-LEDs in the 400-700 nm range. The telemetric laser pointer is used to illuminate the analyzed spot in the red (655 nm). A supercontinuum laser (360 - 1000 nm, 10 mW optical power, SAMBA-UV, LEUKOS) provides the white illumination for RIS. The UV-C, UV-B, red laser and white emissions are collected using a single quartz lens placed at 45° in the horizontal plane to avoid specular reflection and transported through fiber optics to a CCD spectrometer (200-1000 nm, 1044 channels, 100 µm slit, 3 nm resolution Ocean Insight QEPRO). A stabilized tungsten light source providing IR illumination and filtered out to preserve the low intensity luminescence in the NIR range is sent through a fluoride fiber and optics to the sample surface. The IR emitted signals are collected using a fluoride lens and brought through fluoride fiber optics to a SWIR spectrometer using an InGaAs sensor (1000-2500 nm, 256 channels, 50 µm, 13 nm resolution spectrometer, Avaspec NIR-256 2.5 HSC evo, AVANTES).

The synchronization of the illumination alternation is driven by a homemade electronic sequencer that count the number of acquisitions carried out by the QEPRO spectrometer, ensuring a perfect synchronization between the active illumination and its datacube. As a MS Visual Basic software running on a portable computer through USB connections, i.e. without additional electronics, insure the synchronization of the stage X & Y with the six spectra acquisition and the storage in their respective datacube, the reading of the distance and the control the Z stage to keep all the system in focus.

Such optimized optical components and geometry allows collecting acceptable UV-Vis-NIR and SWIR spectra despite the short collection time (e.g. 20 ms and 80 ms respectively). Due to the low intensity of the signals, PL spectra are better acquired in the dark or attenuated light. The scanner delivers in a single pass six datacubes containing all spectra at each pixel: XRF, photoluminescence in the UV-Vis-NIR under excitation at at 250 nm, 365 nm, and 655 nm and reflectance in the Vis-NIR and SWIR ranges.

Data processing

Data formats

The hyperspectral datacubes (XRF, UV-PL at 255/365 nm, NIR-PL at 655 nm and RIS) are stored in EDF format (ESRF Data Format) during scanning since it was the native format for data

visualization and investigation using the PyMCA software package[19]. A global consensus of the cultural heritage MA-XRF and hyperspectral communities towards a common data format has not yet emerged, but the structured and "self-describing" format Hierarchical Data Format version 5 (HDF5)[20] is arising as a very convenient option. For the instrument presented in this article, conversion from EDF format to HDF5 files is achieved after acquisition. Conversion towards other data formats (ENVI dataset, SPECTRONON dataset, etc…) is also possible.

Preprocessing operation

The usual preprocessing operation related to the acquisition of such dataset are realized through homemade Python routines, and available upon request to the corresponding author. Data stitching of multiple scans and correction for small misalignments of the entire datacube are realized through an interactive GUI, while removal of spectral artefacts such as spurious emission lines in the supercontinuum laser and normalization operation of the RIS datacube are carried out with in-line command. Correction for intrinsic luminescence[21] (Kubelka-Munk) and wavelength to energy Jacobian transformation for the emission spectra[22] can also be integrated into the preprocessing workflow of the datacube, again with home-written Python scripts.

Processing software

The MAXRF dataset is first visualized and explored through the versatile and broadly acknowledged PyMCA software initially designed for the processing of XRF spectra. The Region Of Interest (ROI) tool allows displaying the MAXRF acquired maps, for a quick display of the different element distributions over the map by spectral ROI selection, or to show the mean spectrum of a selection of point in the map. The fast linear fitting of the entire dataset enables the quick extraction and display of the different elemental maps. In addition, a basic display and coupled analysis of the other dataset (LIS and RIS) can be achieved thanks to PyMCA ROI Imaging Tool by loading stacks of data of the same shape. When several stacks of data are loaded, a master/slave interaction allows the user to select a spatial region across one map and this region will be selected on the other stacks of data. The mean spectral signature of the region over all the loaded dataset can be displayed, allowing association and visualization of spectral features from the different spectroscopic methods. The dataset acquired with the scanner presented here are particularly well suited for this operation as each dataset feature the same size, spatial resolution and are aligned, i.e. to each pixel correspond a set of XRF, FORS and PL signatures.

To process the RIS and LIS datasets according to usual trends of spectral unmixing in the field of cultural heritage it is possible to use different software, such as ENVI (Harris)[23], SPECTRONON (RESONON)[24], or DataHandlerP[25], the first one being proprietary and the latter two open source. General workflows of spectral unmixing involves dimensional reduction of the dataset, endmembers selection and abundance estimation of the selected or found endmembers[11,14,26]. The different endmembers and their distributions can then be compared with spectral database to identify materials.

Case study

The scanning operation is exemplified on an anonymous test painting dated from the 18th century, which has already been intensively studied in the frame of the development of emerging nuclear methods for forensics in Arts[27] (Fig. 4). The painting is an untitled oil on canvas composition measuring 32 cm x 23 cm, depicting a rural landscape, with a cliff and trees on the left side and few houses around a lake with two small characters on the bottom. Most of the composition is devoted to the depiction of sky at sunset, with various shades of blue, pink, and yellow. Curators from the National Center for Research and Restauration in French Museums (C2RMF) suggested that such a style could correspond to a French school composition of the 17th-18th century. The instrument described here was used to scan the painting with a 400-µm resolution and 80 milliseconds of dwell time for a total scanning time of 8 hours, with the X-Ray generator operating at 40 kV, 0.5 mA. In Fig. 5 are presented elemental maps obtained after the MA-XRF scanning operation. The elemental maps of Pb, Hg, Fe, As, and Sb shows that original composition is mainly painted with pigments such as lead white $(PbCO_3)_2{\cdot}Pb(OH)_2$, vermilion (HgS), iron oxide ($FeO{\cdot}OH$ and Fe_2O_3), orpiment (As_2S_3) and Naples yellow ($Pb_2Sb_2O_7$)[28]. A focus is made on a specific area (red insert on Fig.4), which went under an undated restoration operation, covering what seems to be a church steeple or a tower. The restoration operation appears to have been carried out with a mix of various pigments typical of the 19th and the 20th century: cadmium yellow (CdS) and cadmium sulfo-selenide red (CdS + CdSe), titanium white (TiO_2), and zinc white (ZnO) pigments[28]. Various elemental maps from the selected area are shown in Fig. 6, Pb-L, Pb-M, Hg-L, Cd-L, Fe, Zn, Ti, Se, all shown in linear scale. The Pb and Hg maps show the abundancy of these elements in the original composition, and Cd, Zn, Ti and Se maps clearly display the composition of the restauration area.

All spectra, in Vis-NIR and SWIR ranges, were calibrated using a Spectralon® SRT-MS-050 reference target. Reflectance signatures from different areas are presented in Fig. 7. Inspection of elemental map tends to indicate that the yellow tint of the sky is made out of a mix of Orpiment[28] due to the presence of As, Naples yellow[28] due to the presence of Sb, although reflectance spectrum of this area does not seems to correspond to such a mix. This spectral signature could correspond to the varnish and painting material combination. The restored area display a very specific signature with two sharp absorption front, with inflexion point at 500 nm and 580 nm respectively, with a straight plateau in-between. This shape can be the result of a mix of yellow pigment (Cadmium yellow, Chromium Yellow) and very little red pigment such as Cadmium red, which would be coherent with the distribution maps of such elements seen before (Fig. 6). A comparison between the reflectance spectrum of the restored area and a simulated spectrum of a Chromium Yellow and Cadmium Red mix, derived from Kubelka-Munk theory[29–31] is shown in Fig. 7. b. The actual reflectance spectrum and the simulated one display very similar shape, with a slight shift of 7 nm, corroborating the possible pigment identification from XRF data only.

Exploration of the UV-365nm LIS dataset reveal different emission characteristic of various materials. ROI spectral distribution of certain signals observed are shown in Fig. 8 with their associated spectral signatures. Large band centered around 500 nm is characteristic of aged organic material emission such as binders and varnishes [32,33], whereas on the restauration area, with presumably more recent varnish or no varnish at all and different binder, this large band is not present. The restored area display a very specific luminescence signature that can be

associated to emissions of modern materials, presumably Cadmium and Zinc based pigments[34,35]. Looking closely at Fig. 8.b and c, the shape of the restauration area observed is different compared to the MA-XRF results. Indeed, the generated maps are display of emission signals from varnishes fluorescence but also from aforementioned pigments combined with varnish absorption, this also being an example of how challenging interpretation of LIS can be.

The RIS-SWIR dataset provide information regarding the nature of binders and varnishes used[18,36–38]. The SWIR datacube was processed using ENVI software. The global image in Mininum Noise Fraction in the hourglass wizard clearly show distinct MNF components in the painting, especially for the restored part, that are barely distinguished in XRF or PL (Fig. 9.a and 9.b). The SWIR spectrum of the original composition and of the restored area are presented in Fig 10.a. The distribution of specific band are presented in Fig. 10.c. and Fig. 10. e. To obtain these maps, the SWIR dataset was loaded into ROI Imaging Tool widget of PyMCA, selecting spectral Region of Interest, with Background subtraction PyMCA feature, by drawing a straight line between the spectral ROI limits, and using inverted greyscale, so that stronger absorption bands would appear brighter than a smaller absorption bands. One can observe a signal at 1450 nm (Fig. 10.b), attributed to hydroxyl (-OH) stretching from hydrocerussite[39], which makes sense as the associated distribution map of this signal (Fig. 10.c) follows the one of Pb distribution (Fig. 6). We can also observe a doublet at 1707 nm and 1735 nm (Fig. 10.d), that is present only for the area of the original composition. As the restored area display a more recent varnish layer or no varnish at all, we can assume that this signal can be attributed to the varnish, which is coherent with results from litterature, where this spectral signature can be found in NIR spectra of different varnishes[18,37].

As briefly discussed previously, one can easily see that the instrument presented here generated large datasets from techniques that differ in interpretation, meaning that the exploration of the results requires broad knowledge, not to say expertise, in very different domains. That interpretation is user dependent, meaning that different user could come up with different results based on their experience and knowledge. Moreover, this operation of interpretation can be very time consuming, consideration the very large amount of data generated.

Thus, new approaches can be necessary to explore the dataset and identify the materials probed: data fusion can be considered as the most promising approach. From the work of Llinas et al. [40], Ramos et al. [41] identify two major strategies suitable to be used with such datasets: data level fusion, also called low-level fusion, and feature level fusion, also called mid-level fusion. In low-level fusion, the raw data are fused, and the fused dataset are considered as a single meta-spectra datacubes. In mid-level fusion, the fusion is realized on the most relevant features of each dataset, introducing a previous step of variable selection. They applied both procedures to XRF and Raman spectral dataset of different ochre pigments in order to classify them, and showed that the fused dataset allowed a more accurate classification of these pigments compared to using the XRF or Raman dataset only. Alfeld et al. [42] fused MAXRF and RIS datasets from two different instruments, an operation that needed a computational spatial alignment of the datasets, and performed t-SNE clustering on this joined dataset. The authors observed that the t-SNE classification of the fused dataset allowed a better visualization of the results, as the generated clusters highlights the presence of sub-layers surfaces.

As the instrument presented here generates spatially aligned dataset with the same spatial resolution, analytical workflow based on data fusion can be considered as of great interest of development. Indeed, it could allow to visualize and explore the relationship existing between pigments, binder and varnishes for each pixels of the generated maps. Moreover, a relative notion of stratigraphy could be visualized as MA-XRF and RIS-SWIR probe the matter with a relative depth whereas RIS-Vis-NIR and LIS only reach the first opaque surface encountered. Data fusion processing could thus reveal new information regarding the layered organization of the studied area.

Conclusion and perspectives

To the authors knowledge, the instrument described here constitutes the first instrument dedicated to the study of cultural heritage that delivers six datasets (MAXRF, RIS Vis-NIR, RIS SWIR, UV-LIS at 255 nm, UV-LIS at 365 nm and NIR-LIS at 655nm) in a single pass. These datasets are naturally aligned and with the same resolution, constituting a single datacube that can be process as one, or separately. A wide range of materials generally encounter in cultural heritage fields can thereby be probed in a non-invasive and non-destructive way. Application of this instrument was exemplified on an anonymous painting and the exploration of the generated datasets allowed to visualize and characterize the materials of a restored area. Among the perspectives related to the use of this instrument, the development of routines algorithms and automated process workflow for the rapid identification of materials coupling the various signatures obtained after a scanning operation is currently in progress.

Figures

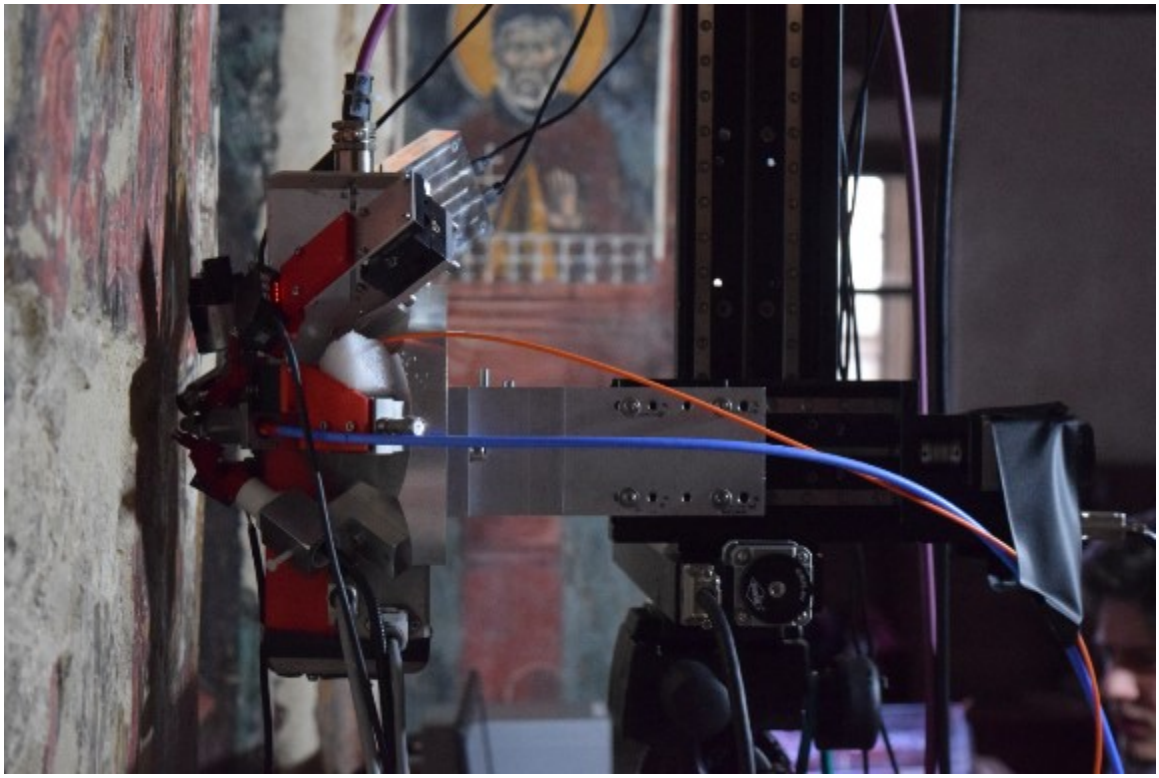

Figure 1: Multi-sensor scanner in operation on the field on a mural painting.

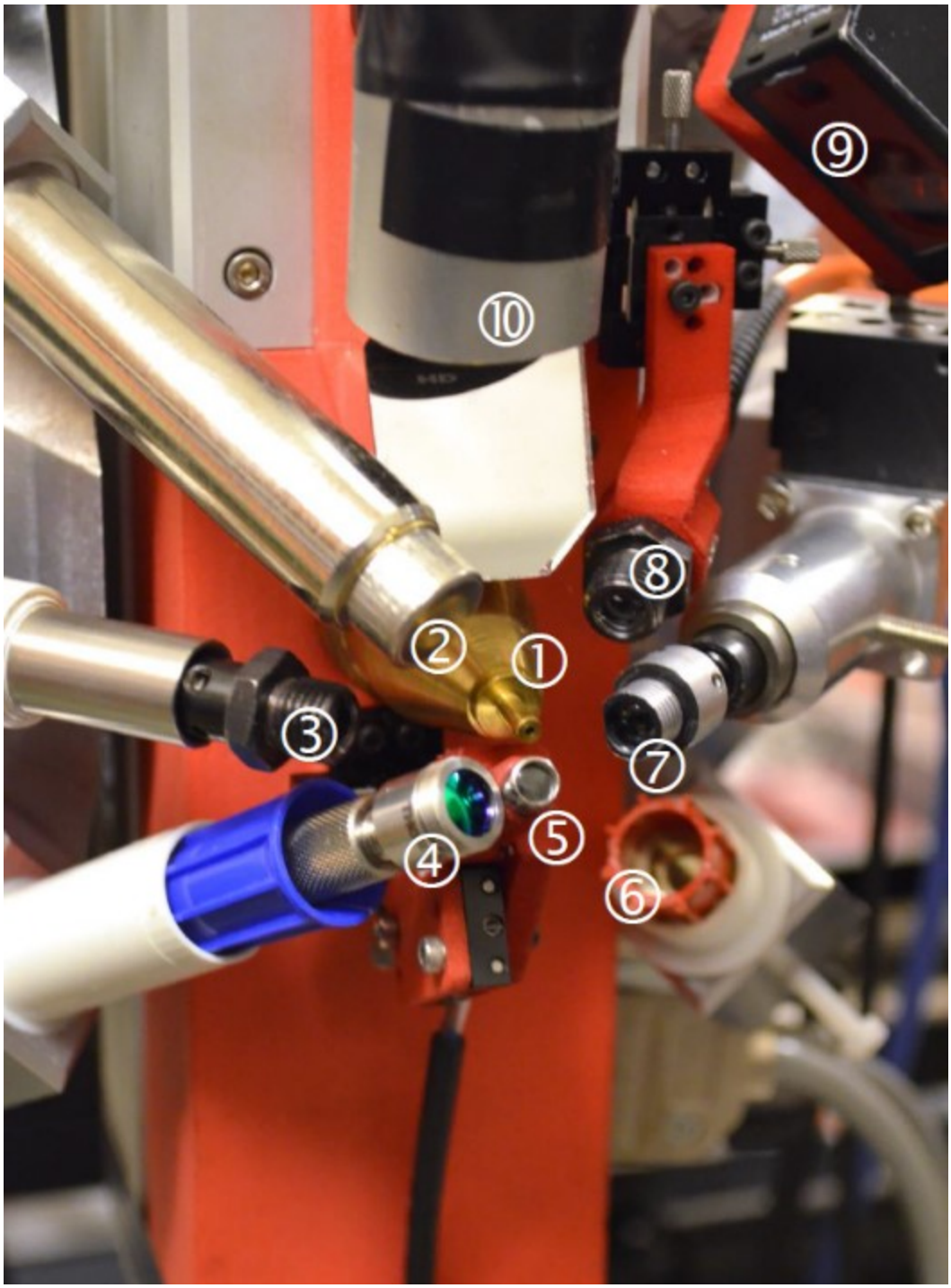

Figure 2: Close up of the analytical head showing the implementation of RS and PL system ① X-Ray collimator ② X-Ray detector ③ SWIR illumination ④ SWIR collection ⑤ UV 250-nm ⑥ White Laser ⑦ UV-Vis-NIR collection ⑧ UV 365-nm ⑨ Telemetric red laser ⑩ Camera

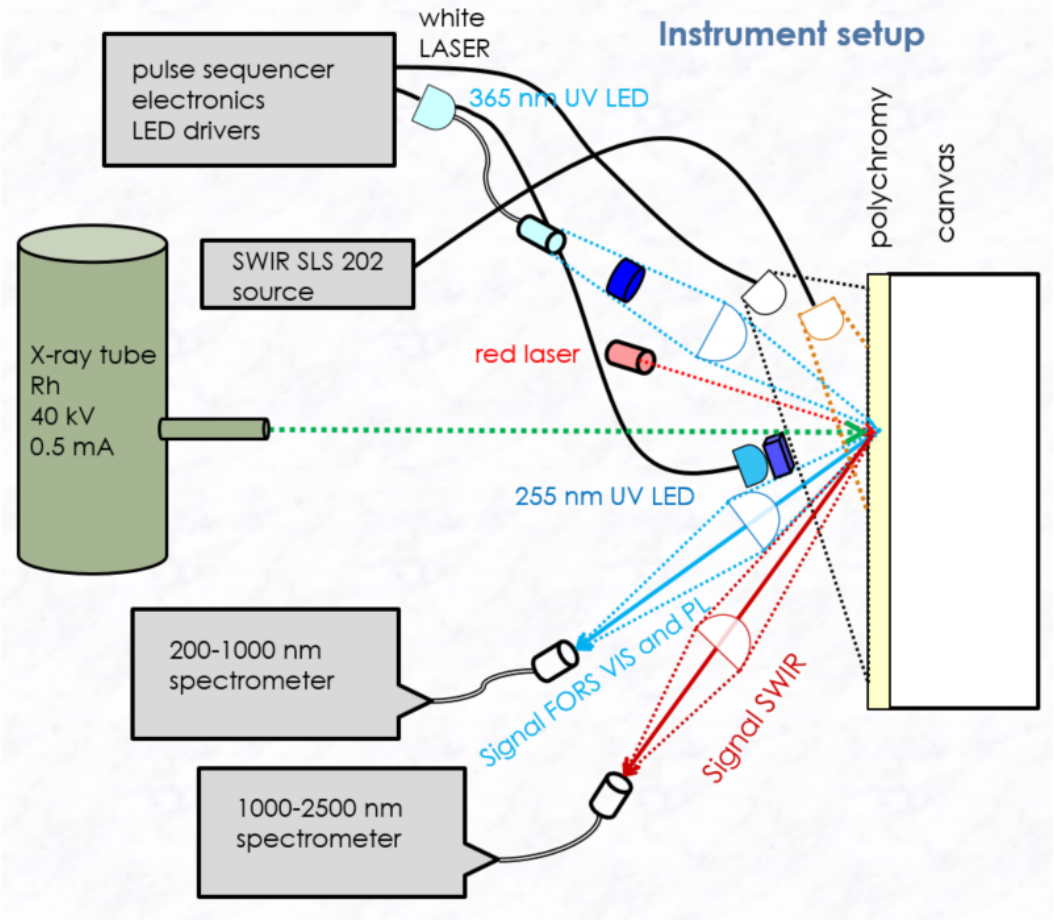

Figure 3: Diagram of the system showing the excitation sources, fiber optics, UV bandpass filter, collimating and collecting lenses, and spectrometers

Figure 4: Test painting, untitled and anonymous composition on canvas. The red dotted squared corresponds to the scanned area.

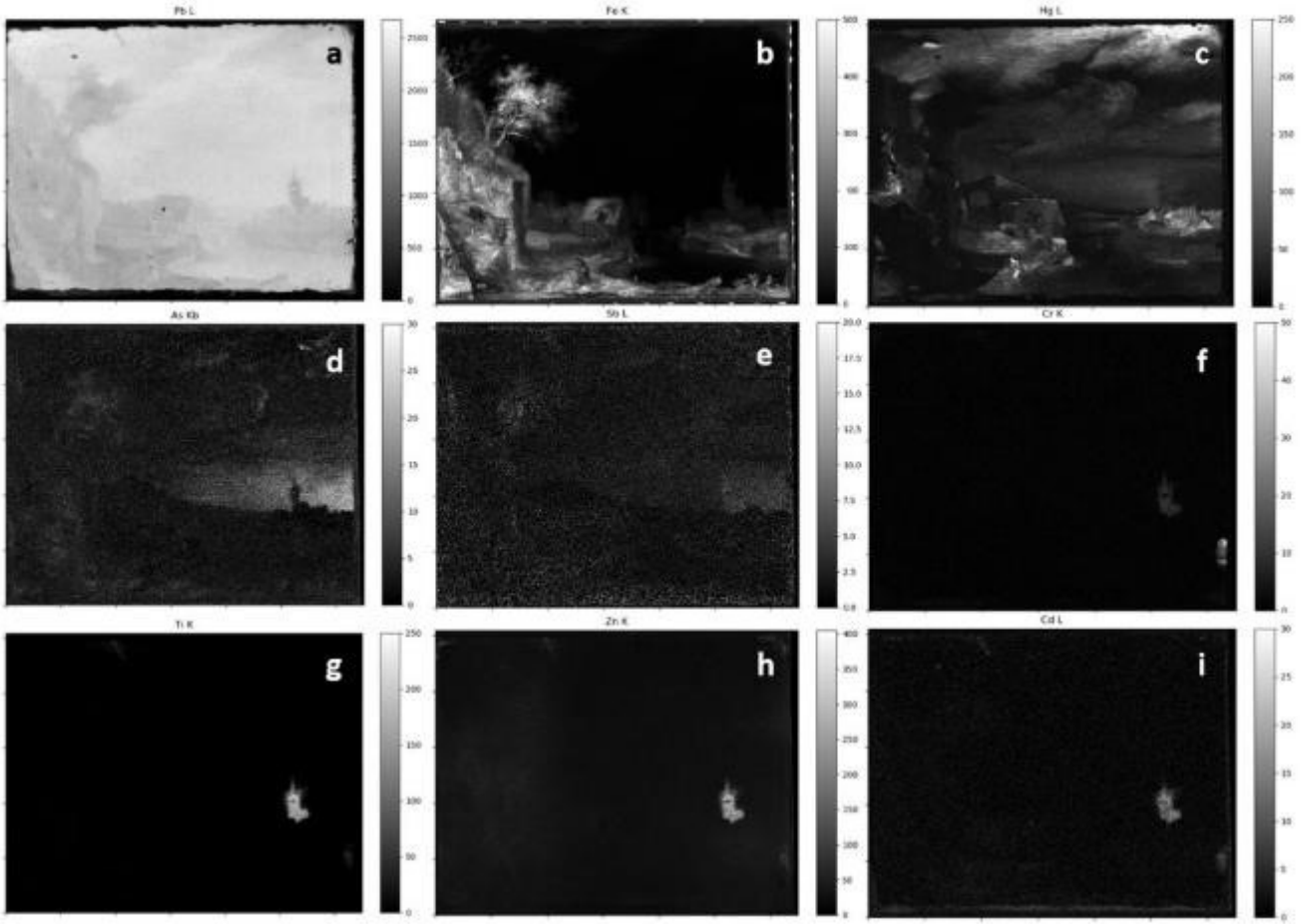

Figure 5: MAXRF elemental maps: a) Pb-L, b) Fe, c) Hg-L, d) As-Kb, e) Sb-L, f) Cr, g) Ti, h) Zn, i) Cd-L, all shown in linear scale. See text for comments.

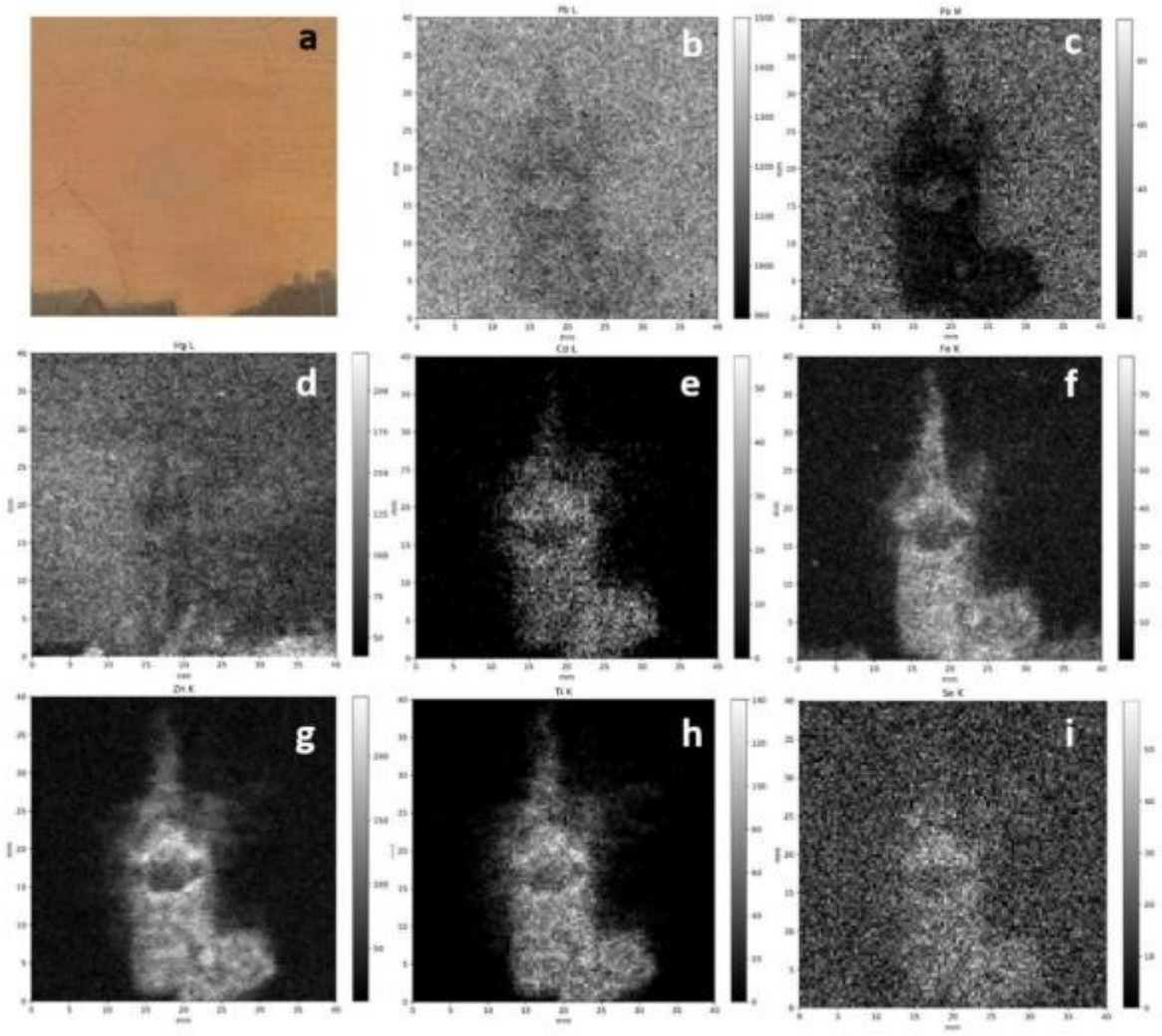

Figure 6: MAXRF elemental maps of the scanned area: a) Visible Image of the area, b) Pb-L, c) Pb-M, d) Hg-L, e) Cd-L, f) Fe, g) Zn, h) Ti, i) Se. See text for comments.

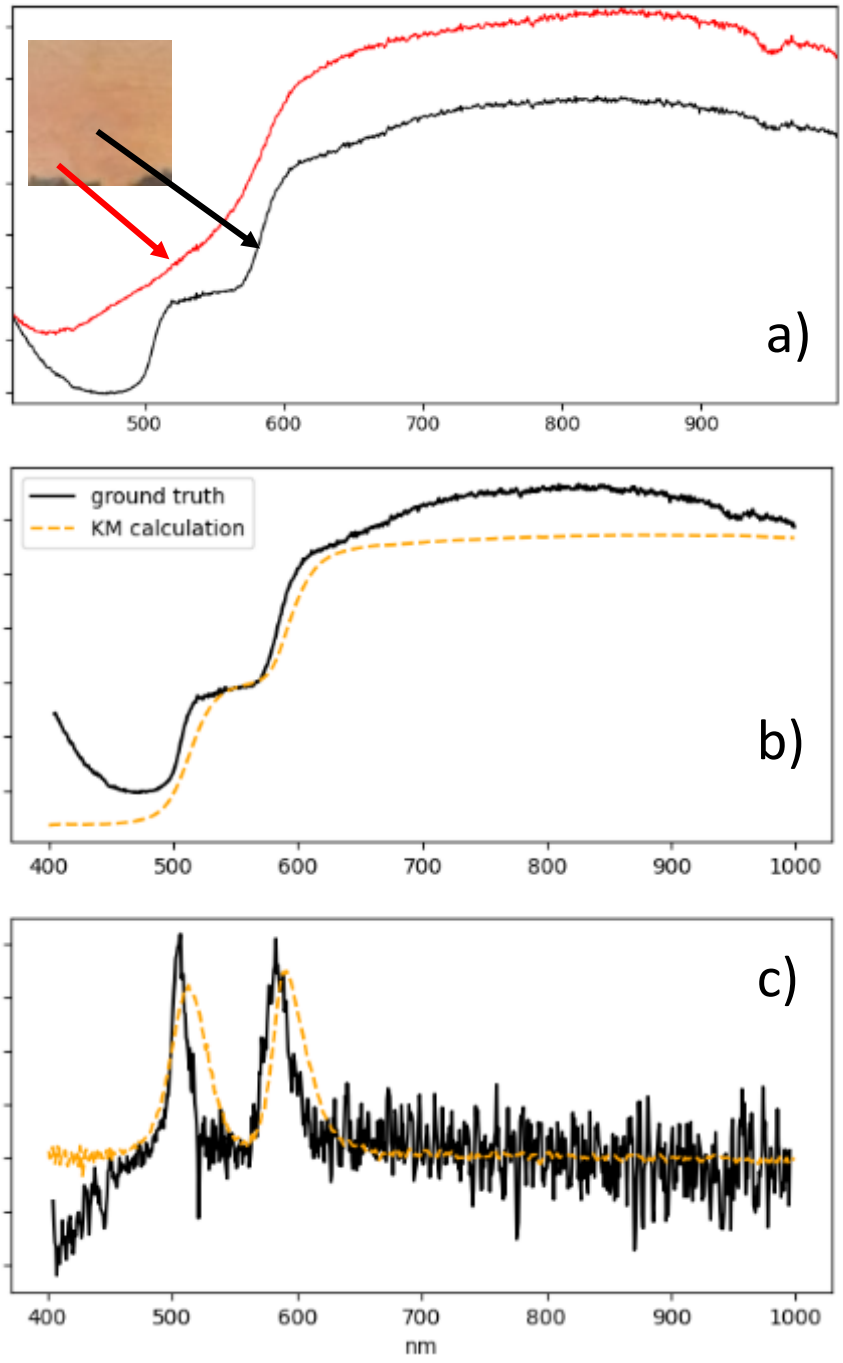

Figure 7: a) Reflectance signature Vis-NIR of the original composition (red), and restored area (black) b) Reflectance signature of the restored area and simulated spectrum derived from Kubelka-Munk theory, with a mix ratio 0.98/0.02 of chromium yellow and cadmium red c) First derivative of the reflectance spectrum of the restored area and the simulated spectrum.

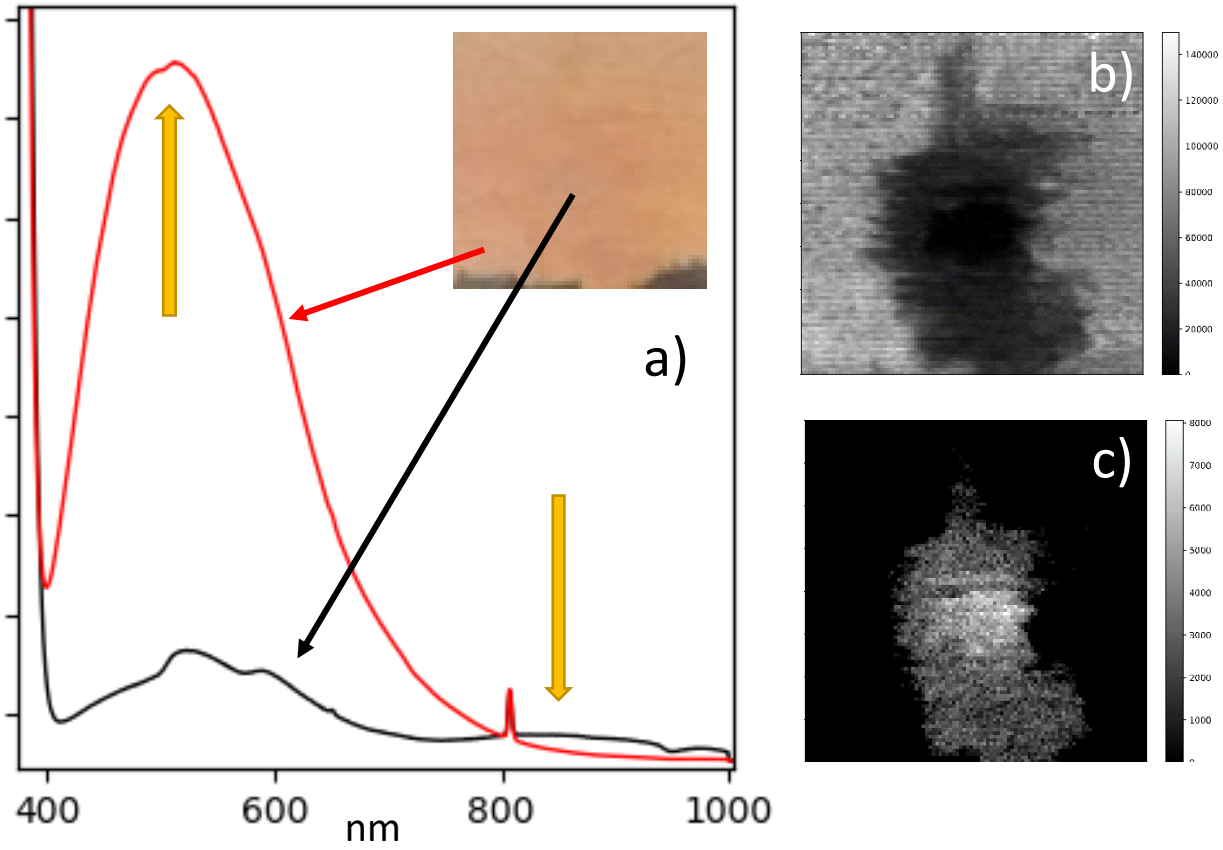

Figure 8: a) Emission spectra of the original composition (red) and restored area (black) b) distribution map of the large band of luminescence observed centered at 500 nm, attributed to organic materials such as binder and varnish c) Distribution map of the large band of luminescence observed between 750 nm and 900 nm, attributed to Cadmium and Zink based pigments.

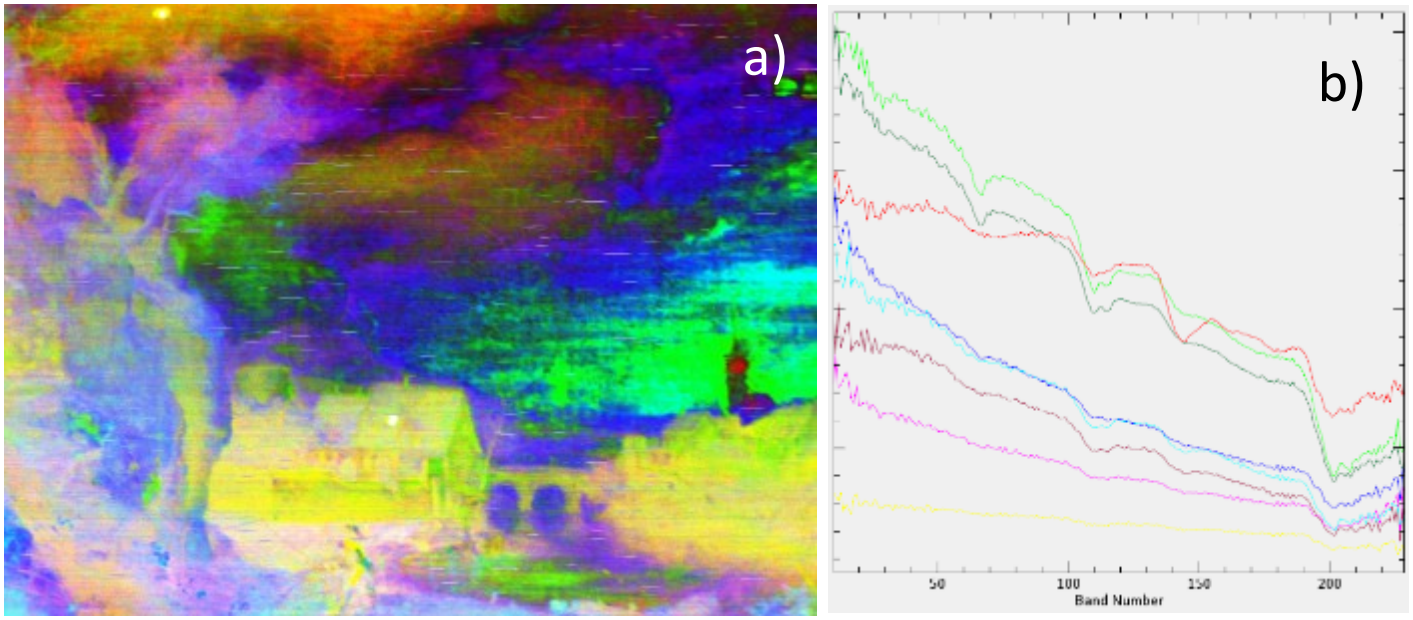

Figure 9: a) RGB display on the RIS SWIR map of the first three MNF components contribution b) Plot of the 8 first MNF components of the RIS SWIR datacube.

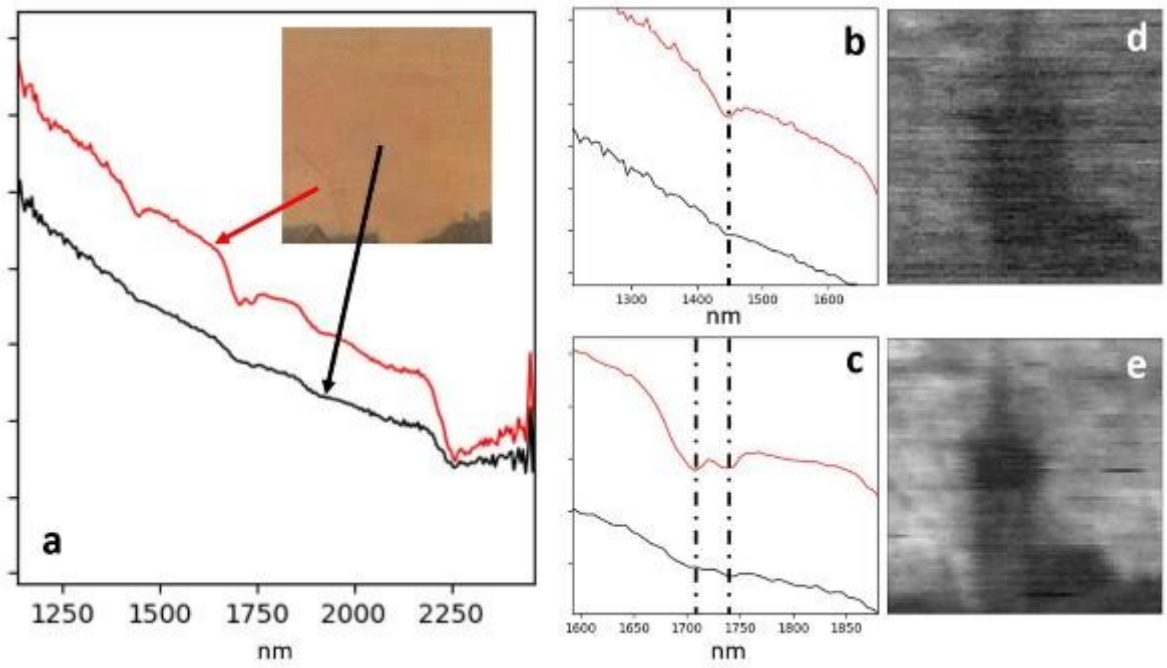

Figure 10: a) Reflectance signature SWIR of the original composition (red), and restored area (black) b) Details of reflectance signature showing an absorption band at 1450 nm attributed to hydroxyl (-OH) stretching from hydrocerussite and d) distribution map of this absorption band. c) Details of reflectance signature showing doublet at 1707 nm and 1735 nm attributed to the varnish and e) distribution map of this absorption band.

References

(1) Alfeld, M.; Janssens, K.; Dik, J.; de Nolf, W.; van der Snickt, G. Optimization of Mobile Scanning Macro-XRF Systems for the in Situ Investigation of Historical Paintings. *J. Anal. At. Spectrom.* **2011**, *26* (5), 899. https://doi.org/10.1039/c0ja00257g.

(2) Hocquet, F.-P.; Calvo del Castillo, H.; Cervera Xicotencatl, A.; Bourgeois, C.; Oger, C.; Marchal, A.; Clar, M.; Rakkaa, S.; Micha, E.; Strivay, D. Elemental 2D Imaging of Paintings with a Mobile EDXRF System. *Anal Bioanal Chem* **2011**, *399* (9), 3109–3116. https://doi.org/10.1007/s00216-010-4281-8.

(3) Alfeld, M.; Pedroso, J. V.; van Eikema Hommes, M.; Van der Snickt, G.; Tauber, G.; Blaas, J.; Haschke, M.; Erler, K.; Dik, J.; Janssens, K. A Mobile Instrument for in Situ Scanning Macro-XRF Investigation of Historical Paintings. *J. Anal. At. Spectrom.* **2013**, *28* (5), 760. https://doi.org/10.1039/c3ja30341a.

(4) Romano, F. P.; Caliri, C.; Nicotra, P.; Di Martino, S.; Pappalardo, L.; Rizzo, F.; Santos, H. C. Real-Time Elemental Imaging of Large Dimension Paintings with a Novel Mobile Macro X-Ray Fluorescence (MA-XRF) Scanning Technique. *J. Anal. At. Spectrom.* **2017**, *32* (4), 773–781. https://doi.org/10.1039/C6JA00439C.

(5) Alberti, R.; Frizzi, T.; Bombelli, L.; Gironda, M.; Aresi, N.; Rosi, F.; Miliani, C.; Tranquilli, G.; Talarico, F.; Cartechini, L. CRONO: A Fast and Reconfigurable Macro X-Ray Fluorescence Scanner for in-Situ Investigations of Polychrome Surfaces. *X-Ray Spectrometry* **2017**, *46* (5), 297–302. https://doi.org/10.1002/xrs.2741.

(6) Ravaud, E.; Pichon, L.; Laval, E.; Gonzalez, V.; Eveno, M.; Calligaro, T. Development of a Versatile XRF Scanner for the Elemental Imaging of Paintworks. *Appl. Phys. A* **2016**, *122* (1), 17. https://doi.org/10.1007/s00339-015-9522-4.

(7) Pouyet, E.; Barbi, N.; Chopp, H.; Healy, O.; Katsaggelos, A.; Moak, S.; Mott, R.; Vermeulen, M.; Walton, M. Development of a Highly Mobile and Versatile Large MA-XRF Scanner for in Situ Analyses of Painted Work of Arts. *X-Ray Spectrom* **2021**, *50* (4), 263–271. https://doi.org/10.1002/xrs.3173.

(8) Alfeld, M.; Janssens, K. Strategies for Processing Mega-Pixel X-Ray Fluorescence Hyperspectral Data: A Case Study on a Version of Caravaggio's Painting Supper at Emmaus. *J. Anal. At. Spectrom.* **2015**, *30* (3), 777–789. https://doi.org/10.1039/C4JA00387J.

(9) Moreau, R.; Brunel-Duverger, L.; Pichon, L.; Moignard, B.; Gourier, D.; Calligaro, T. Application of a MA-XRF/RIS/PL Scanner to Paintwork Studies. *Eur. Phys. J. Plus* **2023**, *138* (1), 16. https://doi.org/10.1140/epjp/s13360-022-03604-8.

(10) Ricciardi, P.; Delaney, J. K.; Glinsman, L.; Thoury, M.; Facini, M.; de la Rie, E. R. Use of Visible and Infrared Reflectance and Luminescence Imaging Spectroscopy to Study Illuminated Manuscripts: Pigment Identification and Visualization of Underdrawings; Pezzati, L., Salimbeni, R., Eds.; Munich, Germany, 2009; p 739106. https://doi.org/10.1117/12.827415.

(11) Delaney, J. K.; Ricciardi, P.; Glinsman, L. D.; Facini, M.; Thoury, M.; Palmer, M.; Rie, E. R. de la. Use of Imaging Spectroscopy, Fiber Optic Reflectance Spectroscopy, and X-Ray Fluorescence to Map and Identify Pigments in Illuminated Manuscripts. *Studies in Conservation* **2014**, *59* (2), 91–101. https://doi.org/10.1179/2047058412Y.0000000078.

(12) Delaney, J. K.; Thoury, M.; Zeibel, J. G.; Ricciardi, P.; Morales, K. M.; Dooley, K. A. Visible and Infrared Imaging Spectroscopy of Paintings and Improved Reflectography. *Herit Sci* **2016**, *4* (1), 6. https://doi.org/10.1186/s40494-016-0075-4.

(13) de Viguerie, L.; Rochut, S.; Alfeld, M.; Walter, P.; Astier, S.; Gontero, V.; Boulc'h, F. XRF and Reflectance Hyperspectral Imaging on a 15th Century Illuminated Manuscript: Combining

Imaging and Quantitative Analysis to Understand the Artist's Technique. *Herit Sci* **2018**, *6* (1), 11. https://doi.org/10.1186/s40494-018-0177-2.
(14) Radpour, R.; Gates, G. A.; Kakoulli, I.; Delaney, J. K. Identification and Mapping of Ancient Pigments in a Roman Egyptian Funerary Portrait by Application of Reflectance and Luminescence Imaging Spectroscopy. *Herit Sci* **2022**, *10* (1), 8. https://doi.org/10.1186/s40494-021-00639-5.
(15) Elias, M.; Chartier, C.; Prévot, G.; Garay, H.; Vignaud, C. The Colour of Ochres Explained by Their Composition. *Materials Science and Engineering: B* **2006**, *127* (1), 70–80. https://doi.org/10.1016/j.mseb.2005.09.061.
(16) Cloutis, E.; MacKay, A.; Norman, L.; Goltz, D. Identification of Historic Artists' Pigments Using Spectral Reflectance and X-Ray Diffraction Properties I. Iron Oxide and Oxy-Hydroxide-Rich Pigments. *Journal of Near Infrared Spectroscopy* **2016**, *24* (1), 27–45. https://doi.org/10.1255/jnirs.1198.
(17) Gonzalez, V.; Gourier, D.; Calligaro, T.; Toussaint, K.; Wallez, G.; Menu, M. Revealing the Origin and History of Lead-White Pigments by Their Photoluminescence Properties. *Anal. Chem.* **2017**, *89* (5), 2909–2918. https://doi.org/10.1021/acs.analchem.6b04195.
(18) Vagnini, M.; Miliani, C.; Cartechini, L.; Rocchi, P.; Brunetti, B. G.; Sgamellotti, A. FT-NIR Spectroscopy for Non-Invasive Identification of Natural Polymers and Resins in Easel Paintings. *Anal Bioanal Chem* **2009**, *395* (7), 2107–2118. https://doi.org/10.1007/s00216-009-3145-6.
(19) Solé, V. A.; Papillon, E.; Cotte, M.; Walter, Ph.; Susini, J. A Multiplatform Code for the Analysis of Energy-Dispersive X-Ray Fluorescence Spectra. *Spectrochimica Acta Part B: Atomic Spectroscopy* **2007**, *62* (1), 63–68. https://doi.org/10.1016/j.sab.2006.12.002.
(20) Collette, A. *Python and HDF5*, First edition.; O'Reilly: Beijiing, 2014.
(21) Verri, G.; Clementi, C.; Comelli, D.; Cather, S.; Piqué, F. Correction of Ultraviolet-Induced Fluorescence Spectra for the Examination of Polychromy. *Appl Spectrosc* **2008**, *62* (12), 1295–1302. https://doi.org/10.1366/000370208786822296.
(22) Mooney, J.; Kambhampati, P. Get the Basics Right: Jacobian Conversion of Wavelength and Energy Scales for Quantitative Analysis of Emission Spectra. *J. Phys. Chem. Lett.* **2013**, *4* (19), 3316–3318. https://doi.org/10.1021/jz401508t.
(23) *Image Processing & Analysis Software | Geospatial Image Analysis Software | ENVI®*. https://www.l3harrisgeospatial.com/Software-Technology/ENVI (accessed 2023-03-09).
(24) *Hyperspectral Scanning System | Imaging Software | Resonon*. https://resonon.com/software (accessed 2023-03-09).
(25) *DataHandlerP*. SourceForge. https://sourceforge.net/projects/datahandlerp/ (accessed 2023-03-09).
(26) Delaney, J. K.; Dooley, K. A.; Radpour, R.; Kakoulli, I. Macroscale Multimodal Imaging Reveals Ancient Painting Production Technology and the Vogue in Greco-Roman Egypt. *Sci Rep* **2017**, *7* (1), 15509. https://doi.org/10.1038/s41598-017-15743-5.
(27) Calligaro, T.; Banas, A.; Banas, K.; Radović, I. B.; Brajković, M.; Chiari, M.; Forss, A.-M.; Hajdas, I.; Krmpotić, M.; Mazzinghi, A.; Menart, E.; Mizohata, K.; Oinonen, M.; Pichon, L.; Raisanen, J.; Siketić, Z.; Šmit, Ž.; Simon, A. Emerging Nuclear Methods for Historical Painting Authentication: AMS-14C Dating, MeV-SIMS and O-PTIR Imaging, Global IBA, Differential-PIXE and Full-Field PIXE Mapping. *Forensic Science International* **2022**, *336*, 111327. https://doi.org/10.1016/j.forsciint.2022.111327.
(28) *Artists' Pigments: A Handbook of Their History and Characteristics*; Feller, R. L., Roy, A., FitzHugh, E. W., Berrie, B. H., Eds.; National Gallery of Art: Washington, 1986.
(29) Kubelka, P.; Munk, F. An Article on Optics of Paint Layers. 16.

(30) Kubelka, P. New Contributions to the Optics of Intensely Light-Scattering Materials Part I. *J. Opt. Soc. Am.* **1948**, *38* (5), 448. https://doi.org/10.1364/JOSA.38.000448.
(31) Liang, H. Advances in Multispectral and Hyperspectral Imaging for Archaeology and Art Conservation. *Appl. Phys. A* **2012**, *106* (2), 309–323. https://doi.org/10.1007/s00339-011-6689-1.
(32) de la Rie, E. R. Fluorescence of Paint and Varnish Layers (Part II). *Studies in Conservation* **1982**, *27* (2), 65–69. https://doi.org/10.1179/sic.1982.27.2.65.
(33) Thoury, M.; Elias, M.; Frigerio, J. M.; Barthou, C. Nondestructive Varnish Identification by Ultraviolet Fluorescence Spectroscopy. *Appl Spectrosc* **2007**, *61* (12), 1275–1282. https://doi.org/10.1366/000370207783292064.
(34) Cesaratto, A.; D'Andrea, C.; Nevin, A.; Valentini, G.; Tassone, F.; Alberti, R.; Frizzi, T.; Comelli, D. Analysis of Cadmium-Based Pigments with Time-Resolved Photoluminescence. *Anal. Methods* **2014**, *6* (1), 130–138. https://doi.org/10.1039/C3AY41585F.
(35) Artesani, A.; Bellei, S.; Capogrosso, V.; Cesaratto, A.; Mosca, S.; Nevin, A.; Valentini, G.; Comelli, D. Photoluminescence Properties of Zinc White: An Insight into Its Emission Mechanisms through the Study of Historical Artist Materials. *Appl. Phys. A* **2016**, *122* (12), 1053. https://doi.org/10.1007/s00339-016-0578-6.
(36) Dooley, K. A.; Lomax, S.; Zeibel, J. G.; Miliani, C.; Ricciardi, P.; Hoenigswald, A.; Loew, M.; Delaney, J. K. Mapping of Egg Yolk and Animal Skin Glue Paint Binders in Early Renaissance Paintings Using near Infrared Reflectance Imaging Spectroscopy. *Analyst* **2013**, *138* (17), 4838. https://doi.org/10.1039/c3an00926b.
(37) Dooley, K. A.; Coddington, J.; Krueger, J.; Conover, D. M.; Loew, M.; Delaney, J. K. Standoff Chemical Imaging Finds Evidence for Jackson Pollock's Selective Use of Alkyd and Oil Binding Media in a Famous 'Drip' Painting. *Anal. Methods* **2017**, *9* (1), 28–37. https://doi.org/10.1039/C6AY01795A.
(38) de Viguerie, L.; Pladevall, N. O.; Lotz, H.; Freni, V.; Fauquet, N.; Mestre, M.; Walter, P.; Verdaguer, M. Mapping Pigments and Binders in 15th Century Gothic Works of Art Using a Combination of Visible and near Infrared Hyperspectral Imaging. *Microchemical Journal* **2020**, *155*, 104674. https://doi.org/10.1016/j.microc.2020.104674.
(39) Delaney, J. K.; Dooley, K. A.; van Loon, A.; Vandivere, A. Mapping the Pigment Distribution of Vermeer's Girl with a Pearl Earring. *Herit Sci* **2020**, *8* (1), 4. https://doi.org/10.1186/s40494-019-0348-9.
(40) Llinas, J.; Hall, D. An Introduction to Multi-Sensor Data Fusion. *ISCAS '98. Proceedings of the 1998 IEEE International Symposium on Circuits and Systems (Cat. No.98CH36187)*. IEEE. Monterey, CA, USA 1998.
(41) Ramos, P. M.; Ruisánchez, I.; Andrikopoulos, K. S. Micro-Raman and X-Ray Fluorescence Spectroscopy Data Fusion for the Classification of Ochre Pigments. *Talanta* **2008**, *75* (4), 926–936. https://doi.org/10.1016/j.talanta.2007.12.030.
(42) Alfeld, M.; Pedetti, S.; Martinez, P.; Walter, P. Joint Data Treatment for Vis–NIR Reflectance Imaging Spectroscopy and XRF Imaging Acquired in the Theban Necropolis in Egypt by Data Fusion and t-SNE. *Comptes Rendus Physique* **2018**, *19* (7), 625–635. https://doi.org/10.1016/j.crhy.2018.08.004.